IOP Publishing New J. Phys. 26 (2024) 083022 https://doi.org/10.1088/1367-2630/ad6bb6

New Journal of Physics
The open access journal at the forefront of physics

Deutsche Physikalische Gesellschaft DPG
IOP Institute of Physics

Published in partnership with: Deutsche Physikalische Gesellschaft and the Institute of Physics

OPEN ACCESS

RECEIVED
15 July 2024

ACCEPTED FOR PUBLICATION
6 August 2024

PUBLISHED
20 August 2024

Original Content from this work may be used under the terms of the Creative Commons Attribution 4.0 licence.

Any further distribution of this work must maintain attribution to the author(s) and the title of the work, journal citation and DOI.

PAPER

Correlated qubit coherences stimulated by thermal energy

N Etehadi Abari*, A A Rakhubovsky and R Filip

Department of Optics, Palacký University, 17. Listopadu 12, 771 46 Olomouc, Czech Republic
* Author to whom any correspondence should be addressed.

E-mail: najme.ettehadi@gmail.com, rakhubovsky@optics.upol.cz and filip@optics.upol.cz

Keywords: quantum coherence, correlated qubit coherence, thermally-induced coherences, Dicke model, quantum Fisher information

Supplementary material for this article is available online

Abstract

Quantum coherence, the ability of a system to be in a quantum superposition of pure states, is a distinct feature of quantum mechanics that has no direct analog in classical mechanics. Quantum states that possess coherence efficiently outperform their classical counterparts in fundamental science and practical applications, including quantum metrology, computation, and simulation. Generation of coherence without the need to employ strong classical drives remains a challenging and not yet experimentally explored task. Beyond individual thermally-induced coherences already proposed for different experiments, correlated quantum coherences of multiple qubits represent a new target. We prove that correlated qubit coherence emerges thermally stimulated from incoherent states in hybrid superconducting and solid-state systems comprising non-interacting qubits coupled only via Dicke-type interaction to a shared thermal mechanical oscillator, exhibits coherences beyond the Tavis–Cummings coupling and, moreover, can be advantageous in quantum sensing.

1. Introduction

In the classical description of a physical system, it is in principle possible to assign perfectly certain values to the system's configuration parameters. Possible uncertainties are associated, in classical physics, with the lack of knowledge of the exact state of the system and are the subject of statistical mechanics and fields alike. In contrast to that, in quantum mechanics, even perfect determination of the state of a system yields *pure* states that can exhibit statistical uncertainties in the form of e.g. the celebrated Heisenberg principle. Consequently, quantum mechanics allows the existence of *coherent quantum superpositions* in such pure states. The ability to create quantum coherent superpositions of relevant basis quantum states is a contributing factor in a multitude of quantum applications including, e.g. quantum metrology [1, 2], communication and cryptography [3, 4], simulation and computing [5–7]. Correspondingly, there exists a substantial effort to quantify quantum coherence [8–13] and study the ways of its creation (see e.g. [14, 15] for reviews).

However, much less is understood and experimentally tested about the operational mechanisms of quantum coherence generation. The paradigmatic approach to generating coherent superpositions of energy basis states typically includes strong coherent and classical driving of the target system. Without the drive, the system itself normally tends to equilibrate to its environment and reach a thermal state, with the latter being merely an incoherent mixture of the energy eigenstates. Therefore, the coherent drive has to compete with the thermalization process and hence the drive strength is a necessity. It has recently been demonstrated, however, that a properly engineered interaction between a system of interest and its thermal environment is capable of generating steady-state coherences [16] in the absence of a coherent drive. The quantum coherence rises from specific coherent interactions with an environment or between sub-systems open to the environment. The powerful drive-less approach has been further studied and developed in [17–25]. A related question of whether transient dynamics can autonomously generate coherence of a qubit coupled to a thermal mechanical oscillator found an affirmative answer in [26]. Moreover, it was shown that increasing the initial temperature of the mechanical oscillator can surprisingly have a positive effect on the amount of generated coherence. Recently, for autonomous quantum thermodynamics, such investigation was focused

© 2024 The Author(s). Published by IOP Publishing Ltd on behalf of the Institute of Physics and Deutsche Physikalische Gesellschaft

to entanglement of interacting qubits between baths with asymmetric temperatures [27, 28], eventually created and enhanced by the joint weakly coupled thermal bath [29, 30] and possibly extendable to many qubits [31–34].

Here, we tackle a more challenging problem of autonomous generation of multi-qubit quantum coherences between different qubits provided by only a coupling to a single thermal oscillator in a star configuration. We show, differently, that starting with fully incoherent states, a much greater correlated quantum coherence emerges [35] already in a symmetric configuration during transient dynamics from only coherent interaction with a single thermal oscillator and persists under relevant thermalization. When the correlated coherence is non-vanishing, although entanglement can be small or even zero, the entire coherence in the system is no longer stored locally and must exist within the correlations between the non-interacting subsystems. Within a certain limit, an increase in the temperature of the mechanical oscillator has a positive effect on the different types of coherence of the qubits. Specifically, we observe different thermally induced correlated coherences due to the counter-rotating terms of the Dicke interactions, eventually combined with local coherences for the composite interactions [16–25, 36], not available in a simpler Tavis–Cummings model without counter-rotating coupling terms. To illustrate the practical applicability of the generated coherence, we analyze quantum sensing of an overall qubit phase and show that the quantum Fisher information of the qubits grows with the increasing temperature of the mechanical oscillator. It overcomes schemes based on an asymmetrical thermal excitation of two qubits coupled by energy-conserving interaction [27–30, 32], that exhibits vanishing Fisher information even if they exhibit correlated coherence.

Motivated by recent progress at the superconducting and solid-state quantum platforms, we study a symmetrical configuration where two (or a larger number of) qubits, not coupled directly to each other, are each coupled to a common mechanical oscillator. In recent years such hybrid systems comprising both two-level systems and harmonic oscillators attracted significant attention [37–39]. Indeed, chaining together subsystems of a fundamentally different nature by means of controllable interfaces allows one to take advantage of the strengths of the individual subsystems. In particular, in the so-called electromechanical systems where superconducting qubits are coupled to motion of a mechanical oscillator [40–47], the qubit can be used to facilitate creation of exotic quantum states of the mechanical oscillator. Complementary, the mechanical oscillator provides a means for the upconversion of the qubit's quantum state to the telecom wavelengths, necessary for efficient long-distance quantum communication. Another example of similar synergy is spin-mechanical systems such as NV-centers coupled to mechanical motion via strain, stress, or magnetic fields [48–52]. Alternatively, mechanical oscillator can be coupled to quantum dots [53–55], or similar coupling can be observed in trapped ions [56, 57], hybrid atom-optomechanical or electro-optomechanical setups [38, 58–61].

Inspired by these experimental possibilities, our study showcases a counterintuitive phenomenon of fully autonomous emergence of correlated coherence in qubits from totally incoherent states. Importantly, the qubits do not interact with each other directly but instead are coupled only via a mediating thermal mechanical oscillator. We test our findings on systems including two and three qubits coupled to a shared mechanical mode and prove that the coherence persists under relevant damping. In practice, such generation of coherence may have applications in quantum information tasks where a coherent joint drive of qubits is not accessible or may be strongly unwanted because of undesired side effects of such drive. To verify an impact in an application, we analyze sensing capability for the collective phase estimation by the qubits using the Fisher information enhanced by the thermally-induced correlated coherences. Our study thus facilitates the development of fully autonomous correlated coherence generation in hybrid systems with potential applications in quantum technology and thermodynamics.

2. Results

2.1. Model and correlated coherence

The simplest system we consider consists of two qubits coupled to a mechanical oscillator (MO) (figure 1(a)). Such a model can be experimentally realized in hybrid electromechanical devices, where qubits are coupled to the mechanical mode capacitively, or via magnetic flux and electromotive interaction [37, 45, 62–64]. Another suitable platform for studying qubit-mechanical interaction at a quantum level is represented by the spin-mechanical devices in which the mechanical oscillator can couple to the spin of the NV centers or quantum dots in solid-state systems [50, 53, 65].

Considering a Dicke-type interaction [66, 67], typical for the superconducting and solid-state platforms described above, our system of interest with two identical qubits ($N = 2$) can be described by the following Hamiltonian ($\hbar = 1$)

$$H = \omega_{\rm m} a^\dagger a + \frac{1}{2}\sum_{i=1}^{2}\omega_{q_i}\sigma_{z_i} + \sum_{i=1}^{2} g_{x_i}\sigma_{x_i}\left(a + a^\dagger\right), \tag{1}$$

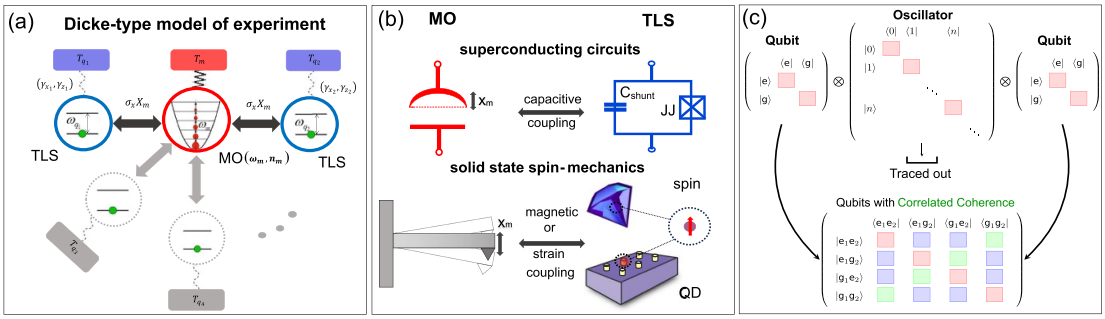

Figure 1. (a) Schematic diagram of a hybrid system comprising a mechanical oscillator (MO) with frequency $\omega_{\rm m}$ interacting via Dicke-type coupling with two or more two-level systems (TLSs or qubits) with the transition frequencies ω_{q_i}. MO is coupled at a rate $\gamma_{\rm m}$ to a bath at temperature $T_{\rm m}$ corresponding to mean occupation $n_{\rm th}$. At the same time, MO can be cooled down and initialized in the thermal state with a different thermal occupation $n_{\rm m} \neq n_{\rm th}$. Qubits also interact with their individual baths and undergo the damping and dephasing at rates $\gamma_{x_i}, \gamma_{z_i}$. (b) Possible experimental implementations of hybrid qubit-mechanical systems [48]. Above: capacitive coupling of a movable membrane to a superconducting qubit (JJ: Josephson junction, $C_{\rm shunt}$: shunting capacity), below: magnetic or strain coupling of a cantilever to an NV-center or a quantum dot. (c) Conceptual scheme of the correlated coherence buildup. The initially incoherent states (diagonal in the energy bases) of the qubits and the oscillator transforms (after tracing out the mechanical oscillator) into a state of two qubits that can have both local coherence (blue squares) and correlated coherence (green squares).

where the first two terms describe the free evolution of the mechanical oscillator and the qubits, respectively. We denote a and $a^\dagger$ the annihilation and creation operators of the MO with frequency $\omega_{\rm m}$, while ω_{q_i} is the transition frequency of the ith qubit described by the Pauli matrices σ_{μ_i} $(\mu = x, y, z;\, i = 1, 2)$. The last sum in equation (1) describes the interaction between the MO and the qubits, parametrized by coupling rates g_{x_i}. For the most part, we assume two identical qubits at resonance with MO: $\omega_{q_1} = \omega_{q_2} = \omega_{\rm m}$, and the coupling rates equal: $g_{x_1} = g_{x_2} = g_0$. The impact of unequal frequencies and coupling rates is studied in sections S1 and S7. In the rotating wave approximation, the counter-rotating terms in the Hamiltonian vanish, and the resulting interactions can be described using the Tavis–Cummings model. Importantly, the T–C model, while creating correlated coherences between the qubits, does not produce quantum states that are capable of increasing the resolution of collective phase shift measurement (see section S5).

In order to evaluate the thermally-induced effects in the system, we estimate its quantum state $\hat{\rho}(t)$ as a function of time. The system starts in a product state where the MO is initialized in a thermal state with mean occupation $n_{\rm m}$ while two qubits are prepared in their ground states $|g_i\rangle$ $(i = 1, 2)$. The MO's initial temperature can be made lower than the one of its bath by using cavity or feedback cooling [68]. In order to find the evolution of the density matrix, we solve numerically either von Neumann master equation, for a closed system, or the Lindblad or Bloch–Redfield master equation for an open system (see section 4 for details). An approximate solution for short-time unitary dynamics of the closed system is in section S4. For the case of an open system, we consider the mechanical oscillator to be coupled to its environment (characterized by mean occupation $n_{\rm th}$) at rate $\gamma_{\rm m}$, and the qubits to experience damping and dephasing at rates γ_{x_i} and γ_{z_i} with the qubits environments being in vacuum. The state of the two qubits is then obtained from $\hat{\rho}(t)$ by tracing out the degrees of freedom of the MO: $\hat{\rho}_{\rm qq}(t) = {\rm Tr}_{\rm m}(\hat{\rho}(t))$.

For the analysis of the coherence of the qubits, we use two measures of quantum coherence. First is the relative entropy of coherence [9, 11] that for an arbitrary state $\hat{\pi}$ reads

$$\mathcal{C}_{rel}(\hat{\pi}) = S\left(\hat{\pi}^{\rm diag}\right) - S(\hat{\pi}), \tag{2}$$

where $S(\hat{\pi}) \equiv -{\rm Tr}[\hat{\pi}\ln\hat{\pi}]$ is von Neumann entropy, and $\hat{\pi}^{\rm diag} = \sum_i \langle i|\hat{\pi}|i\rangle\, |i\rangle\langle i|$ is the density matrix $\hat{\pi}$ with off-diagonal elements removed. Second, the quantum correlated coherence [12], which for the state of two qubits reads:

$$\mathcal{C}_{\rm cc}\left(\hat{\rho}_{\rm qq}\right) = \mathcal{C}_{\rm rel}\left(\hat{\rho}_{\rm qq}\right) - \mathcal{C}_{\rm rel}\left(\hat{\rho}_{q_1}\right) - \mathcal{C}_{\rm rel}\left(\hat{\rho}_{q_2}\right), \tag{3}$$

where $\hat{\rho}_{q_1(q_2)}(t) = {\rm Tr}_{q_2(q_1)}[\hat{\rho}_{\rm qq}(t)]$ is the state of the first (second) qubit obtained by partial trace over degrees of freedom of the second (first) one.

Hereinafter, we will refer to $\mathcal{C}_{\rm rel}(\hat{\rho}_{\rm qq})$ as the *total* relative entropy of coherence in order to distinguish it from the local relative entropy of coherence $\mathcal{C}_{\rm rel}(\hat{\rho}_{q_i})$ of individual qubits. The total relative entropy of two-qubit coherence in equation (2) describes the overall amount of local coherence together with the one present in their correlation. Therefore, we use the correlated coherence (3) that discards the local quantum relative entropies of coherence, to distinguish them [12]. When $\mathcal{C}_{\rm rel}(\hat{\rho}_{qq}) = \mathcal{C}_{\rm cc}(\hat{\rho}_{qq})$, no coherence is present

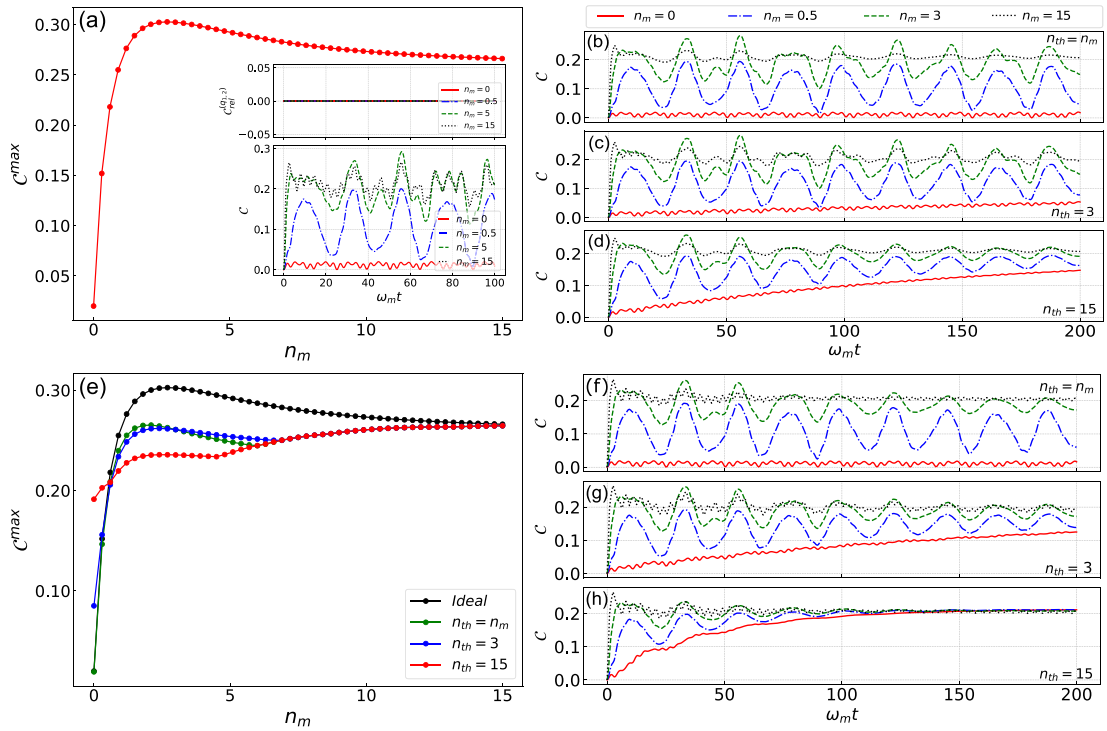

Figure 2. Correlated coherence $\mathcal{C} = \mathcal{C}_{cc} = \mathcal{C}_{rel}$ in the system of two qubits induced by thermal fluctuations of a mechanical oscillator (Dicke-Type model). (a) and (e) Maximally attainable amount of quantum correlated coherence (total entropy of coherence) $\mathcal{C}^{max}$ as a function of initial mechanical occupation n_m. (a) Ideal case of unitary evolution according to the Dicke model (1). Inset plots show total coherence $\mathcal{C}(t)$ as a function of time and the vanishing of the local relative entropy of coherence $\mathcal{C}_{rel}^{(q_{1,2})}$. (e) Maximally attainable coherence in an open system (black line reproduces the results of panel (a) for comparison). (b)–(h) Open-system simulation of the qubits coherence as a function of time using different approaches, for different initial thermal occupations n_m and different bath temperature n_{th} of the mechanical oscillator. (b)–(d) Bloch–Redfield master equation-based approach, (f)–(h) Lindblad master equation-based approach. Other parameters are: coherent coupling rates $g_0 \equiv g_{x_1} = g_{x_2} = 0.1\omega_m$, mechanical damping rate $\gamma_m = 10^{-3}\omega_m$, all qubit damping and dephasing rates $\gamma_{x_i,z_i} = 2 \times 10^{-5}\omega_m$ (with $i = 1, 2$).

locally and all the coherence comes from the correlations between the qubits. As our qubit system is considered local, and no qubit communication is relevant in such a scenario, we use correlated coherence as the appropriate quantity instead of more narrow entanglement and broader entropy of coherence.

2.2. Thermally-induced correlated coherence of two qubits

To estimate the capability of a thermal mechanical oscillator to induce correlated coherence in the two-qubit system, we first consider the unitary evolution induced by the Dicke-type Hamiltonian (1). Results of the simulations are in figure 2(a) where we show the maximum attainable values of quantum correlated coherence $\mathcal{C}_{cc}$ and total relative entropy of coherence $\mathcal{C}_{rel}$ as a function of the initial thermal occupation of the mechanical mode, n_m. Besides, the inset plots in figure 2(a) demonstrate the evolution of $\mathcal{C} \equiv \mathcal{C}_{cc} = \mathcal{C}_{rel}$ as functions of time for different values of initial phonon number n_m. We should note that in the absence of coupling term $\propto \sigma_z(a + a^\dagger)$ in the Dicke model, it is not possible to generate local qubit coherences in the system, (see inset plot of figure 2(a) and [26]). In this condition, the quantum correlated coherence would be equal to the total relative entropy of coherence. From panel (a) of figure 2, it is clear that the rising of the initial occupation number of the mechanical mode causes the maximum accessible amount of quantum correlated coherence (total relative entropy of coherence) to increase. There is a range of optimum values for $2 \lessapprox n_m \lessapprox 4$ at which $\mathcal{C}^{max}$, takes the highest values ($\mathcal{C}^{max} \approx 0.30$). Increasing n_m further causes the coherence to saturate at a slightly lower value around $\mathcal{C}^{max} \approx 0.27$.

The thermal environment of the mechanical oscillator plays a twofold role in the creation of the qubits' coherence in our scheme. First, it is instrumental in the preparation of the initial thermal state of the MO, which has a positive effect on the coherence, and second, a fraction of the coherence is dissipated towards this environment and hence lost. Therefore, it is important to also investigate the open-system dynamics including the dissipation of the MO. Our analysis shows that the thermal noise of the oscillator's environment does not break the emergent effect of the correlated coherence. As is seen in figures 2(b)–(h), the maximum values of $\mathcal{C}^{max}$ only get reduced but remain thermally stimulated in the presence of the fixed

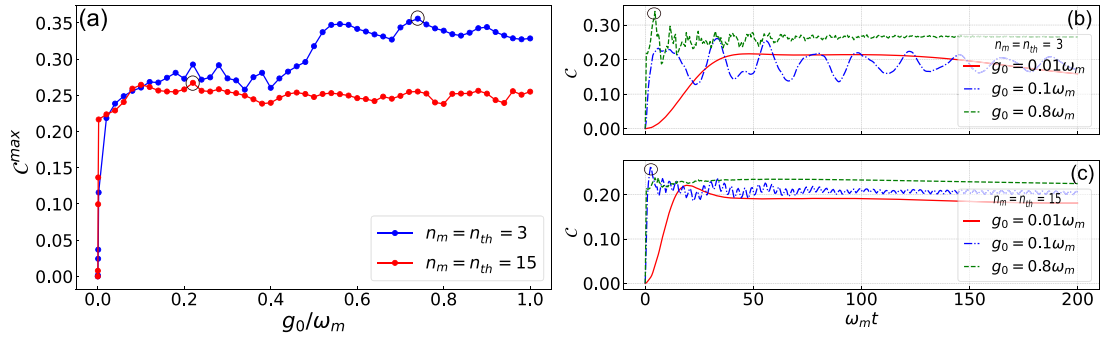

Figure 3. (a) Maximal qubits' coherence as a function of net qubit-mechanical coupling g_0/ω_m for different initial occupation numbers $n_m = n_{th} = 3, 15$ for the time period $t \in [0, 100]$. The black circles indicate the maximum values of $\mathcal{C}^{max}$ which can be reached for strong coupling $g_0/\omega_m \approx 0.74$ when $n_m = n_{th} = 3$ and moderate coupling rate $g_0/\omega_m \approx 0.22$ when $n_m = n_{th} = 15$. (b), (c) Quantum correlated coherence (relative entropy of coherence) as a function of time for different coupling rates when (b) $n_m = n_{th} = 3$ and (c) $n_m = n_{th} = 15$. Black circles specify the maximum attainable of $\mathcal{C}$. Other parameters same as in figure 2.

mechanical damping rate $\gamma_m = 10^{-3}\omega_m$ as well as two-qubit damping and dephasing rates, $\gamma_{x_{1,2}} = \gamma_{z_{1,2}} = 2 \times 10^{-5}\omega_m$. In addition, the maximum values of $\mathcal{C}^{max}$ shift to the higher initial occupations n_m while we increase the thermal phonons. In panels (b)–(d) of figure 2, the time evolution of the qubits' coherence is depicted for the open system dynamics (we have used the Bloch–Redfield approach to extract the final state of the system). As seen, the results are in line with the outcomes of master equation methods (see figures 2(f)–(h)) (there is only a small deviation for higher numbers of n_m around the initial time interval). In figure 2(e), the optimum values of $\mathcal{C}^{max}$ are depicted as a function of the initial occupation n_m for different mechanical thermal noise n_{th} in a time period $t \in [0, 100]$. Additionally, figures 2(f)–(h) illustrates the time evolution of the coherences. For the same damping, we see that the maximum amounts of quantum correlations between two qubits in terms of qubit–qubit coherence increase as a function of the initial phonon number n_m. Starting from the vacuum state of the MO, i.e. $n_m = 0$, we get the higher values for $\mathcal{C}^{max}$ when we increase the temperature of the mechanical bath, i.e. n_{th}. For some values of n_m, $0.6 \lessapprox n_m < 6$, the occupation number of the mechanical bath plays the negative role, while for $n_m \geqslant 6$, $\mathcal{C}^{max}$, becomes independent of n_{th} as well as n_m for sufficiently long time interval. The time evolution plots of figures 2(f)–(h) also show the same results where the quantum coherence is depicted as a function of normalized time $\omega_m t$. The best outcome is obtained for the initial time period and when $n_m = 15$. The independent behavior of $\mathcal{C}^{max}$ with respect to n_{th} in figure 2(e) is consistent with the time evolution results (see panels (f)–(h) of figure 2), where the maximum values of the qubit–qubit coherence are achieved at initial time intervals when the thermal environment can not significantly affect the dynamics of the system. Moreover, $\mathcal{C}$ being independent of initial thermal occupation n_m for long time evolution (see figures 2(b)–(d) and (f)–(h)), could indicate the outcomes of steady-state solution where the system performs autonomously of initial conditions. Curiously, from figure 2(e) it follows that for certain temperatures of the bath (e.g. $n_{th} = 15$), pre-cooling of the mechanical oscillator only reduced achievable coherence.

The effect of the coupling constant g_0 on qubit–qubit coherence is shown in figure 3. As is seen, for smaller thermal phonon number $n_m = n_{th} = 3$, we obtained better results for $\mathcal{C}^{max}$ in the strong coupling regime where $g_0 \geqslant 0.5\omega_m$. However, the highest values of coherence for $n_m = n_{th} = 15$ can be attained already for moderate coupling rate $0.1 \leqslant g_0/\omega_m \leqslant 0.3$. Here, we checked the behavior of the maximally attainable coherence parameter for time period $\omega_m t \in [0, 100]$ for the same decoherence parameters as in figure 2. In addition, panels (b) and (c) in figure 3(a) demonstrate the evolution of qubit–qubit coherence $\mathcal{C}$ in time for different thermal phonon numbers $n_m = n_{th} = 3$ and 15 as well as different coupling rates. It is visible that the evolution of $\mathcal{C}$ undergoes faster relaxation towards the steady state for weak and ultra-strong coupling $g_0 = 0.01\omega_m$ and $g_0 = 0.8\omega_m$, respectively, while for the moderate coupling, $\mathcal{C}$ shows the oscillating patterns for a longer time. On the other hand, we can reach greater steady-state values for quantum correlated coherence $\mathcal{C}$, as we increase the two-qubit-mechanical couplings g_0.

Here, we consider a rather simplified case of symmetric Dicke-type resonant coupling of two qubits to a mechanical oscillator. For the study of the effects of other characteristic parameters on qubit–qubit coherence, we refer the reader to sections S1 and S7. In particular, we show that the quantum correlated coherence of the qubits is maximized in this regime compared to cases of detuned qubits ($\omega_{q_i} \neq \omega_m$) or coupling other than the Dicke-type one (e.g. $\propto (\sigma_{x_1} + \sigma_{x_2})X_m$). In terms of damping rates, we also demonstrated that the qubit–qubit coherence is not affected by higher values of the mechanical damping γ_m and it is robust against the qubits decoherence compatible with the state-of-the-art parameters [46, 69].

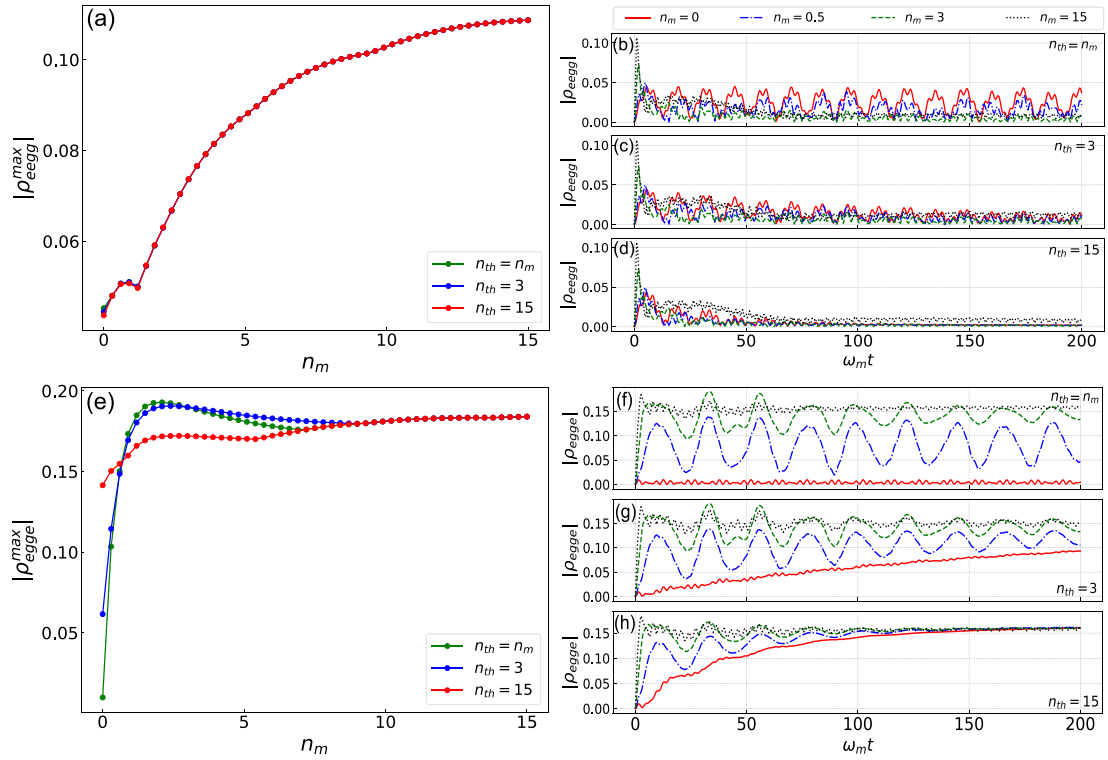

Figure 4. Non-zero off-diagonal elements of the density matrix of the two qubits. (a) and (e) maximal values of the density matrix elements, (a) $|\hat{\rho}^{\max}_{\mathrm{eegg}}|$ and (e) $|\hat{\rho}^{\max}_{\mathrm{egge}}|$ as a function of the initial mechanical occupation number n_{m} for different values of the mechanical environment occupation n_{th}. (b)–(d) and (f)–(h) Time evolution of the matrix elements for different occupations n_{m} and n_{th}. Other parameters same as in figure 2.

2.3. Structure of the density matrix for correlated coherence

As we observed previously, individual qubits in our system show no local coherence in their partial states, but instead, the present coherence originates from the correlations between the two qubits. This indicates the creation of non-classical correlations between the qubits and raises the questions of whether the qubits exhibit entanglement and what is the structure of the density matrix. Of certain interest are the off-diagonal elements of the density matrix of the two qubits. In particular, we evaluate the off-diagonal contributions of the maximally entangled Bell states, $|\Phi_{\pm}\rangle \propto |\mathrm{gg}\rangle \pm |\mathrm{ee}\rangle$ and $|\Psi_{\pm}\rangle \propto |\mathrm{eg}\rangle \pm |\mathrm{ge}\rangle$. Here, $|\mathrm{e,g}\rangle$ are the energy basis states of the qubits: $\sigma_z|\mathrm{e}\rangle = |\mathrm{e}\rangle, \sigma_z|\mathrm{g}\rangle = -|\mathrm{g}\rangle$. These contributions are defined as $|\hat{\rho}_{\mathrm{eegg}}(t)| = |\langle \mathrm{ee}|\hat{\rho}_{\mathrm{qq}}(t)|\mathrm{gg}\rangle|$ and $|\hat{\rho}_{\mathrm{egge}}(t)| = |\langle \mathrm{eg}|\hat{\rho}_{\mathrm{qq}}(t)|\mathrm{ge}\rangle|$. For the Bell states, one has $|\langle \mathrm{ee}|\Phi_{\pm}\rangle\langle\Phi_{\pm}|\mathrm{gg}\rangle| = 1/2$ and $|\langle \mathrm{eg}|\Psi_{\pm}\rangle\langle\Psi_{\pm}|\mathrm{ge}\rangle| = 1/2$. These values apparently constitute the upper boundary of the achievable matrix elements values. Separable pure states that, in the general case, have the form $|x,y\rangle \equiv (\sqrt{x}|\mathrm{e}\rangle + \sqrt{1-x}|\mathrm{g}\rangle)\otimes(\sqrt{y}|\mathrm{e}\rangle + \sqrt{1-y}|\mathrm{g}\rangle)$ (with $0 \leqslant x,y \leqslant 1$) can also have non-zero matrix elements of this kind. Straightforward maximization shows that for the pure separable states $|\langle \mathrm{ee}|x,y\rangle\langle x,y|\mathrm{gg}\rangle| = \sqrt{x(1-x)y(1-y)} \leqslant 1/4$ with the inequality saturated when $x = y = 1/2$. A very similar calculation shows that the same bound is valid also for the matrix elements corresponding to $|\Psi\rangle$. Moreover, it is easy to prove that this bound applies also to mixed separable states.

In figure 4, we show how the maximal values of the density matrix elements $|\hat{\rho}^{\max}_{\mathrm{eegg}}|$ and $|\hat{\rho}^{\max}_{\mathrm{egge}}|$ behave with respect to initial thermal phonon number n_{m} in the case of open system dynamics, with different occupations of the bath. As previously, we consider the cases $n_{\mathrm{th}} = 3, 15$, and $n_{\mathrm{th}} = n_{\mathrm{m}}$. According to figure 4, increasing the initial mechanical occupation has a positive effect on maximal obtainable values of the density matrix elements. In the case of $|\hat{\rho}^{\max}_{\mathrm{eegg}}|$, its increase indicates that the mechanical oscillator mediates a $\sigma_{x_1}\sigma_{x_2}$—type coupling between the qubits with the strength of this interaction positively correlated with the oscillator's initial occupation. On the other hand, the element $|\hat{\rho}^{\max}_{\mathrm{egge}}|$ can rise due to simple quanta hoping between differently occupied oscillators. The element $|\hat{\rho}^{\max}_{\mathrm{eegg}}|$ is an increasing function of n_{m}, while the behavior of $|\hat{\rho}^{\max}_{\mathrm{egge}}|$ in figures 3(b) and (d) is similar to the one of the coherence. Concerning the temporal dynamics, from the inset plots of figure 4, we realize that the maximal values for those elements are attained during the initial transient time interval. Moreover, $|\hat{\rho}_{\mathrm{egge}}(t)|$ tends to saturate around some steady value $|\hat{\rho}_{\mathrm{egge}}| \approx 0.15$ for longer time which would be independent of n_{m}, while $|\hat{\rho}_{\mathrm{eegg}}|$ diminishes fast in time when

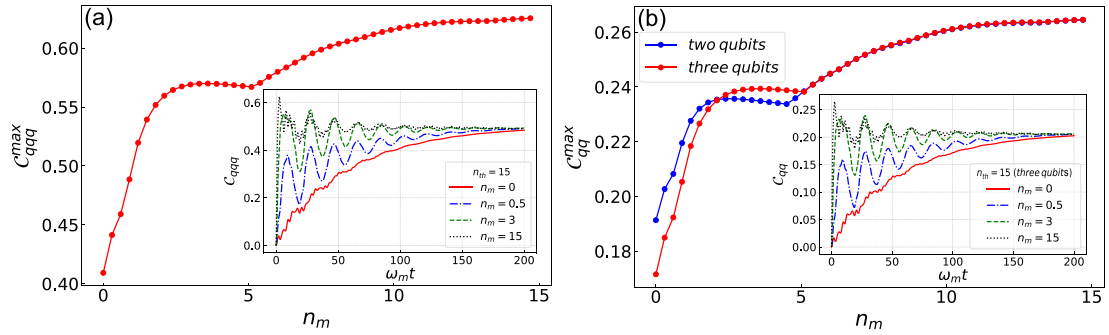

Figure 5. Optimum values of (a) quantum correlated coherence (relative entropy of coherence) $\mathcal{C}^{\max}_{qqq}$ of three qubits and (b) bipartite quantum correlated coherence (relative entropy of coherence) $\mathcal{C}^{\max}_{qq}$ in qubit-mechanical Dicke model with two (blue line) and three (red line) qubits. Inset plots in panels (a) and (b) show the evolution of tripartite as well as bipartite quantum correlated coherence (relative entropy of coherence), respectively. Mechanical environment occupation $n_{\rm th} = 15$, other parameters same as in figure 2.

the thermal phonon $n_{\rm m} = n_{\rm th}$ increases (compare inset plots (c) and (d) of figure 4). By inspection, we see that the off-diagonal elements of the density matrix of the qubits ρ other than $\hat{\rho}_{\rm eegg}, \hat{\rho}_{\rm egge}$ are zero.

On the other hand, the application of specific entanglement measures such as concurrence and negativity to the system of the qubits reveals that the qubits are, in fact, entangled. However, this entanglement is weak, and moreover, decreases with the temperature of the MO, in contrast with coherence which is stimulated by the temperature of the MO. The two qubits appear to be rather strongly entangled with the mechanical oscillator which is indicated by decreased purity of the system of the two qubits, and by negativity. For further details regarding the entanglement of the qubits, we refer the reader to the supplementary materials.

2.4. Thermally-induced correlated coherence of three qubits

As a generalization of our scheme, we consider an additional qubit coupled to the mechanical oscillator. We keep the Dicke model so that the new system Hamiltonian is a direct generalization of equation (1) obtained by extending summation to include the third qubit. In the case of three identical qubits coupled to the mechanical oscillator, the quantum correlated coherence can be defined as a straightforward generalization of equation (3) (see [12]):

$$\mathcal{C}_{\rm cc}\left(\hat{\rho}_{\rm qqq}\right) = \mathcal{C}_{\rm rel}\left(\hat{\rho}_{\rm qqq}\right) - \mathcal{C}_{\rm rel}\left(\hat{\rho}_{q_1}\right) - \mathcal{C}_{\rm rel}\left(\hat{\rho}_{q_2}\right) - \mathcal{C}_{\rm rel}\left(\hat{\rho}_{q_3}\right). \tag{4}$$

After a Dicke-type interaction, the local relative entropy of the coherence of each individual qubit is zero and the quantum correlated coherence acquires its maximum value which is equal to the relative entropy of coherence ($\mathcal{C} = \mathcal{C}_{\rm cc} = \mathcal{C}_{\rm rel}$). The effect of increasing the number of qubits on the quantum correlated coherence of three qubits as well as bipartite quantum correlated coherence has been shown in figures 5(a) and (b), where we consider three identical qubits initialized in the ground state, coupled to a mechanical oscillator, which is initially in the thermal state with mean excitation number $n_{\rm m}$. When the system undergoes dissipation and noise, we studied the transient behavior of the qubits coherence stimulated by initial thermal occupation $n_{\rm m}$ while keeping the thermal occupation of the mechanical bath fixed at $n_{\rm th} = 15$. As is seen in figure 5(b), bipartite quantum correlated coherence $\mathcal{C}^{\max}$ for the three-qubit model behaves similarly as in the two-qubit model in higher values of initial thermal phonon numbers.

In addition, for the three-qubit system, the optimum values of three-qubit-coherence $\mathcal{C}^{\max}_{qqq}$ as a function of $n_{\rm m}$ are shown in figure 5(a). According to [9], the upper bound for the relative entropy of coherence for a $d-$dimensional system is

$$\mathcal{C}_{\rm rel}\left(\hat{\rho}\right) \leqslant \mathcal{S}\left(\hat{\rho}^{\rm diag}\right) \leqslant \ln d. \tag{5}$$

For two qubits with $d = 2^2$, $\mathcal{C}_{\rm cc,rel}{}^{\rm qq} < 0.26 \approx 0.19 \times 2\ln 2$, while for three qubits with $d = 2^3$, we have $\mathcal{C}^{\rm qqq}_{\rm cc,rel} < 0.63 \approx 0.30 \times 3\ln 2$. As expected, by increasing the number of qubits, the ratio $\mathcal{C}_{\rm cc,rel}/\ln d$ improves.

A study of the density matrix elements similar to the one in section 2.3 reveals that the off-diagonal element corresponding to the GHZ state equals zero: $\langle {\rm ggg}|\hat{\rho}|{\rm eee}\rangle = 0$. This indicates that the three-qubit coherence is generated by effective bipartite interactions $\sigma_{(1)}\sigma_{(2)}$ between the qubits, but the effective tripartite interaction $\sigma_{(1)}\sigma_{(2)}\sigma_{(3)}$ is too weak to play a meaningful role in the coherence generation.

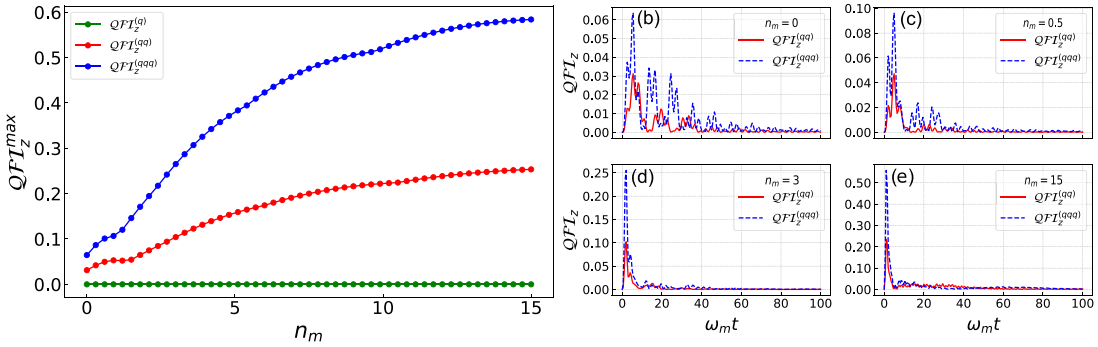

Figure 6. Quantum Fisher information for collective phase estimation using two [red lines] or three [blue] qubits initialized in the state, correspondingly, $\rho_{\rm qq}$ or $\rho_{\rm qqq}$. The nonzero QFI is provided by the correlated coherence of the qubits' state as the local coherence is not generated during the interaction with the oscillator in the Dicke model. The numerical parameters same as in figure 2.

2.5. Quantum Fisher information

The results of the previous sections stimulate an essential question. Can thermally-induced correlated coherence of multiple qubits be used in an application, although the entanglement between these qubits is relatively small? As an illustration that the generated multiqubit coherence can have practical sensing applications we focus on estimation of collective phase applied to all the qubits. Therefore, the sensor's qubits are affected only globally and feel the same phase change which is physically motivated for realistic systems. Here, we evaluate the quantum Fisher information (QFI) [70] of the quantum state of two and three qubits as a function of the mechanical oscillator thermal occupation $n_{\rm m}$. QFI is one of the central figures of merit in quantum metrology [71, 72] providing the ultimate precision attainable by a general measurement with a given quantum state at the input. Here we evaluate QFI for a collective phase estimation described by the generator $H_{\rm meas} = \frac{1}{2}\theta\sum_i \sigma_{z_i}$ performed with the two [or three] qubits initialized in the state $\rho_{\rm qq}$ [or $\rho_{\rm qqq}$] produced by the interaction with the thermal mechanical oscillator. In our setup, prior to the interaction with the mechanical oscillator, the two qubits are assumed initialized in the ground states. As these are eigenstates of σ_{z_i}, invariant under $H_{\rm meas}$, these initial states themselves are not suitable for such measurement. Coupling to a thermal oscillator, however, makes the qubits' state practical for phase detection.

The QFI as a function of the initial occupation of the mechanical oscillator is presented in figure 6. First, we can clearly see that the QFI increases for the larger mechanical oscillator's initial occupation. In contrast to the coherence which, as a function of $n_{\rm m}$ saturates to the value lower than its maximal, the QFI is a steadily increasing function of the initial mechanical temperature. In figures 6(b)–(e), we illustrate the behavior of the QFI as a function of time for different initial mechanical occupations $n_{\rm m}$. The maximal value of QFI is achieved after a short initial transient dynamics. As the occupation $n_{\rm m}$ increases, the height of the initial peak increases, and the duration of the transient leading to the optimal value advantageously decreases. Another important observation comes from comparison of the dependence of the maximal QFI on the number m of the qubits with the classical scaling $\mathrm{QFI}_m \propto m\times \mathrm{QFI}_1$. This expression shows that when using product states of single qubits for phase estimation, the total QFI simply adds. For a single qubit, in the Dicke model, interaction with a thermal MO produces neither coherence nor QFI at all. For two or three qubits, these quantities are non-zero. Importantly, from comparison of results for two and three qubits, it follows that the advantage from the third qubit goes beyond the linear classical scaling. This suggests that the metrological improvement originates from the truly non-classical correlations that emerge through interaction with a thermal mechanical oscillator. We can also see this from the structure of the evolved density matrix of the qubits (section 2.3) where the only non-zero off-diagonal matrix elements are the ones corresponding to the *correlated* coherence.

3. Discussion

We investigated the effects of initial thermal occupation on the coherence of a pair of qubits in the Dicke-type model emerging autonomously from the initial incoherent states of each of the modes. We demonstrated how initial thermal phonons can increase the coherence between two qubits. It is important to note that there is initially no coherence (with respect to the energy basis) in the system, and all the generated coherence emerges as a result of the rectification of the thermal fluctuations by the Hamiltonian interaction in the system. To quantify the qubit–qubit coherence in the system, we used the relative entropy of coherence

and quantum correlated coherence measures. Higher values of quantum correlated coherence (total relative entropy of coherence) can be achieved by increasing the initial thermal phonon number $n_{\rm m}$ and usually emerge during the initial time interval (first few periods of mechanical oscillations). The maximum coherence is gained when the qubits are resonant with the mechanical oscillator. Moreover, the Dicke-type coupling is optimal for maximizing the correlated coherence between the qubits. This is in contrast with the local coherence of individual qubits which requires coupling involving two Pauli matrices ($(\sigma_x+\sigma_z)X_{\rm m}$) to appear [26]. In the Dicke model, no local coherence in the individual quantum states of the qubits is generated. These results are quantitatively confirmed by simulations of the Tavis–Cummings model for moderate qubit-MO couplings (and qualitatively for stronger couplings, see SI). Interestingly, while the numerical amount of coherence generated in the T–C model is close to the coherence in the Dicke model, the T–C model does not increase quantum Fisher information for phase shift measurement. The thermal environment of the mechanical oscillator plays a positive role in generating the qubit–qubit coherence. This is not only by initialization of the MO in a thermal state. Additionally, we observed that by elevating the mechanical bath temperature or equivalently, thermal occupation of the bath $n_{\rm th}$, $\mathcal{C}(t)=\mathcal{C}_{\rm cc}(t)=\mathcal{C}_{\rm rel}(t)$ converges into a steady value more quickly and that steady value is independent of initial thermal phonon $n_{\rm m}$. The hotter MO with $n_{\rm m}=n_{\rm th}$, gave us better results for qubit–qubit quantum coherence in a moderate qubit-mechanical coupling range $g_0=0.1\omega_{\rm m}$, while for smaller $n_{\rm m}=n_{\rm th}$ higher values of $\mathcal{C}(t)$ are obtained for strong coupling regime.

The structure of the density matrix of the qubits points out the effective type of interaction between them. We found that increasing the initial thermal phonon $n_{\rm m}$ can increase the optimum values of both matrix elements $|\hat{\rho}^{\rm max}_{\rm egge}|$ and $|\hat{\rho}^{\rm max}_{\rm eegg}|$. The maximum value of $|\hat{\rho}_{\rm eegg}(t)|$ is attained for an initial time interval, while it diminishes fast in time when we increase the temperature of the mechanical bath. Nevertheless, the time evolution character of $|\hat{\rho}_{\rm egge}(t)|$ is similar to the one of $\mathcal{C}(t)$.

In addition, we investigated the Dicke model with three qubits coupled to a shared MO. Such a system behaves similarly, the thermal mechanical occupation also stimulates coherence between the qubits. This can be seen both in pairwise coherence between the qubits and in tripartite coherence between them. The tripartite coherence $\mathcal{C}_{\rm qqq}$ is closer to the geometric boundary $C<N\ln 2$ attainable in N-qubit system than the bipartite coherence $\mathcal{C}_{\rm qq}$ in Dicke model with only two qubits.

Finally, we have demonstrated an increase of the quantum Fisher information corresponding to linear measurement with the MO's initial temperature increase. We have shown that this result holds for systems with two and three qubits coupling to mechanics. The quantum Fisher information (QFI) is a measure of the sensitivity of a quantum state to small changes in a parameter. For a qubit, assuming interferometric measurement linear in Pauli matrices, the QFI indicates the sensitivity of the qubit state $\hat{\rho}$ with respect to rotations about coordinate axes. Initialization of a qubit in the ground state readily yields maximal QFI with respect to $\sigma_{x,y}$ because the ground state is a coherent superposition of their eigenstates. Simultaneously, QFI with respect to σ_z ($\mathcal{QFI}_z$) is minimal at the ground state, because this state is invariant upon the action of σ_z. Advantageously, the Dicke-type interaction with a thermal mechanical oscillator increases $\mathcal{QFI}_z$ during a short initial time interval yielding a peak in QFI. The peak magnitude is an increasing function of initial mechanical occupation $n_{\rm m}$ as well. Importantly, after adding the third qubit, the QFI strongly increases, beyond classical linear scaling proportional to the number of qubits.

Our studies were, in part, inspired by the rapid development of electromechanical devices [45, 64, 73]. In typical electromechanical systems, the transition frequency of the qubits is normally $\sim$1 GHz, while the mechanical frequency and the coupling rate can be of the order of $\omega_{\rm m}\approx 10$ MHz to 1×10^3 MHz and $g_0\approx$ 1 MHz to 100 MHz [64, 69]. Our proposed protocol is thus within the experimental reach of the electromechanical systems. Another prospective domain is represented by the high-overtone bulk acoustic oscillators that can be coupled to TLSs via piezoelectricity [40, 46] with both TLSs and mechanical oscillators having nearly equal frequencies of the order of few gigahertz.

Application of quantum coherence in the fields of biology [74], quantum sensing [75], quantum thermodynamics [76–78], and quantum non-equilibrium models [79–81] has made it a hot research topic in recent years. For such an application to be successful, proper manipulation and coherence maintenance are crucial. However, it is worth noting that quantum coherence, as a vulnerable quantum property, can be easily disturbed due to the interaction of the system with the environment which leads to decoherence. Generally speaking, a system's decoherence increases as its size does. Therefore, maintaining coherence in larger-scale quantum systems remains a significant challenge. Here, we proposed a model that facilitates the autonomous generation of correlated coherence in systems of multiple qubits in the presence of damping and noise with prospective application in quantum phase sensing. This model is physically accessible and can be manipulated on a larger scale [63, 82–84].

4. Methods

It is possible in electromechanical devices and analogous setups to generate couplings between more than one qubit and a mechanical oscillator [53, 63]. In general, interaction of a system of N qubits with a mechanical oscillator can be described by a Hamiltonian ($\hbar \equiv 1$):

$$H = \frac{\omega_{\rm m}}{2}\left(X_{\rm m}^2 + P_{\rm m}^2\right) + \sum_{i=1}^{N}\frac{\omega_{q_i}}{2}\sigma_{z_i} + \sqrt{2}\sum_{i=1}^{N} g_i\left(\sigma_{x_i}\cos\phi_i\sin\theta_i + \sigma_{y_i}\sin\phi_i\sin\theta_i + \sigma_{z_i}\cos\theta_i\right)X_{\rm m}. \tag{6}$$

Here $X_{\rm m}, P_{\rm m}$ are the dimensionless quadratures of the MO: $[X_{\rm m}, P_{\rm m}] = {\rm i}$. The angles (ϕ_i, θ_i) define the type of coupling between each qubit and the MO.

By considering all the qubits to be identical and for all $\phi_i = 0$ and $\theta_i = \pi/2$, equation (6) transforms into Dicke model in which a bosonic mode is coupled simultaneously to N two-level systems (qubits) [66, 67, 85]. The Dicke-type model with $N = 2$ is also known as a two-qubit Rabi model [86]. The analytical solution of such a scheme, using the Bargmann representation as well as perturbation theory and under some specific assumptions, has been already studied [86–88].

Here, we extract the numerical solution of the two-qubit Rabi model in the presence of dissipation and noise by using the QuTiP package [89]. We assume both qubits to be initialized in ground states while the mechanical oscillator in a thermal state such that the initial state of the tripartite system reads

$$\hat{\rho}(0) = \hat{\rho}_{\rm q_1}(0)\otimes\hat{\rho}_{\rm q_2}(0)\otimes\hat{\rho}_{\rm m}(0) = |g_1\rangle\langle g_1|\otimes|g_2\rangle\langle g_2|\otimes\sum_{k=0}^{\infty}\frac{{n_{\rm m}}^k}{(1+n_{\rm m})^{k+1}}|k\rangle\langle k|, \tag{7}$$

where $|g_i\rangle$ $(i = 1, 2)$ are the ground states of the qubits, $|k\rangle$ is a Fock state of the mechanical oscillator. Mean occupation of the MO equals $n_{\rm m}$ satisfying Bose–Einstein statistics $n_{\rm m} = [\exp(\hbar\omega_{\rm m}/k_{\rm B}T_{\rm m}) - 1]^{-1}$, $k_{\rm B}$ being the Boltzmann constant and $T_{\rm m}$ the effective temperature of the MO.

To investigate the quantum properties of the system such as quantum coherence and quantum entanglement, we need to access the evolved density matrix of the system. This is obtained by numerically solving the von Neumann equation $\dot{\hat{\rho}}(t) = -{\rm i}[H, \hat{\rho}]$ in the ideal case of no decoherence, or the Lindblad master equation

$$\begin{aligned}\dot{\hat{\rho}} = &-{\rm i}\left[H, \hat{\rho}\right] + \frac{\gamma_{\rm m}}{2}\left(n_{\rm th}+1\right)\mathcal{L}\left(a\right)\hat{\rho} + \frac{\gamma_{\rm m}}{2}n_{\rm th}\,\mathcal{L}\left(a^{\dagger}\right)\hat{\rho}\\ &+\sum_{i=1}^{2}\left\{\frac{\gamma_{x_i}}{2}\left(n_{q_i}+1\right)\mathcal{L}\left(\sigma_{+_i}\right)\hat{\rho} + \frac{\gamma_{x_i}}{2}n_{q_i}\,\mathcal{L}\left(\sigma_{-_i}\right)\hat{\rho} + \gamma_{z_i}\left(2n_{q_i}+1\right)\left(\sigma_{z_i}\hat{\rho}\sigma_{z_i} - \hat{\rho}\right)\right\},\end{aligned} \tag{8}$$

in the presence of dissipation and noise. Here, $\mathcal{L}(O)\hat{\rho} \equiv 2O\hat{\rho}O^{\dagger} - (O^{\dagger}O\hat{\rho} + \hat{\rho}O^{\dagger}O)$ denotes the Lindblad superoperator. Furthermore, $\gamma_{\rm m}$, $\gamma_{x_i} = 1/T_1$ and $\gamma_{z_i} = 1/T_2$ $(i = 1, 2)$ represent the mechanical and ith qubit relaxation and dephasing rates, respectively. Occupation of thermal environment of ith qubit is denoted n_{q_i}. For superconducting qubits, to a good accuracy, $n_{q_i} = 0$.

A different approach to look into the dynamics of an open system can be obtained through the Bloch–Redfield method [90, 91]. The method can be applied when there is a weak coupling between a system and the environment such that the Markovian approximation remains valid. The Bloch–Redfield master equation in the Scrödinger picture reads

$$\dot{\hat{\rho}} = -{\rm i}\left[H, \hat{\rho}\right] - \sum_{m}\left[S_m, \Lambda_m\hat{\rho}(t) - \hat{\rho}(t)\,\Lambda_m^{\dagger}\right], \tag{9}$$

where $\hat{\rho}(t)$ is the reduced density matrix of the system and S_m and Λ_m are operators that describe the coupling to the environment. In the Bloch–Redfield approach, the system-bath interaction is defined by the Hamiltonian $H_I = \sum_n S_n B_n$, with S_n being a system operator which acts only on the system degree of freedom while B_n acting only on the degrees of freedom of the environment. In addition, $\Lambda_m = \sum_n \int_0^{\infty} C_{mn}(\tau)S_{n,{\rm int}}(\tau)\,d\tau$, with $C_{mn}(\tau) = {\rm Tr}[B_{m,{\rm int}}(\tau)B_{n,{\rm int}}(0)\hat{\rho}_{\rm env}]$ introducing the bath correlation function, $\hat{\rho}_{\rm env}$ represents the density operator of the bath which is in thermal equilibrium, while $B_{\alpha,{\rm int}}(\alpha = n, m)$ and $S_{n,{\rm int}}$ denotes the bath and system operators, respectively, in the interaction picture.

Once we find the final state of the system, we can easily draw out the information from the quantum aspects of qubit-mechanical interactions such as quantum coherence, entanglement and etc. To quantify the quantum coherence we use the measure of relative entropy of coherence and quantum correlated coherence represented in equations (2) and (3) as well as density matrix elements $|\hat{\rho}_{\rm eegg}|$, $|\hat{\rho}_{\rm egge}|$. In addition, by extending the definition of the quantum correlated coherence and total relative entropy of coherence for

more than two qubits, the study of the behavior of two or more qubits in terms of quantum correlated coherence will be possible.

Quantum Fisher information for a linear measurement $H_{\text{meas}} \propto \sum_i \sigma_{z_i}$ given an initial state ρ can be computed as [92]

$$F_Q(\rho, H_{\text{meas}}) = 2 \sum_{i,j \neq i} \frac{(\lambda_i - \lambda_j)^2}{\lambda_i + \lambda_j} |\langle i|H_{\text{meas}}|j\rangle|^2, \tag{10}$$

where $|i\rangle$ and λ_i denote the eigenvector and corresponding to it eigenvalue of the density matrix ρ. The summation runs over indices for which $\lambda_i + \lambda_j > 0$ $(i \neq j)$.

Data availability statement

All data that support the findings of this study are included within the article (and any supplementary files).

Acknowledgments

We acknowledge the Grant No. 23-06308S of the Czech Science Foundation. R F acknowledges the project 8C22001 (SPARQL) of MEYS Czech Republic and the funding from the European Union's Horizon 2020 research and innovation framework program under Grant Agreement No. 731473 and 101017733. We also acknowledge EU projects H2020-WIDESPREAD-2020-5 project NONGAUSS (951737) under the CSA—Coordination and Support Action and project CZ.02.01.01/00/22_008/0004649 (QUEENTEC) of EU and MEYS Czech Republic.

ORCID iDs

N Etehadi Abari https://orcid.org/0000-0002-2241-0014
A A Rakhubovsky https://orcid.org/0000-0001-8643-670X
R Filip https://orcid.org/0000-0003-4114-6068

References

[1] Giovannetti V, Lloyd S and Maccone L 2011 *Nat. Photon.* **5** 222
[2] Pezzè L, Smerzi A, Oberthaler M K, Schmied R and Treutlein P 2018 *Rev. Mod. Phys.* **90** 035005
[3] Sergienko A V 2018 *Quantum Communications and Cryptography* (CRC Press)
[4] Pirandola S *et al* 2020 *Adv. Opt. Photonics* **12** 1012
[5] Preskill J 1998 *Proc. R. Soc.* A **454** 385
[6] Ladd T D, Jelezko F, Laflamme R, Nakamura Y, Monroe C and O'Brien J L 2010 *Nature* **464** 45
[7] Buluta I and Nori F 2009 *Science* **326** 108
[8] Baumgratz T, Cramer M and Plenio M B 2014 *Phys. Rev. Lett.* **113** 140401
[9] Xi Z, Li Y and Fan H 2015 *Sci. Rep.* **5** 10922
[10] Winter A and Yang D 2016 *Phys. Rev. Lett.* **116** 120404
[11] Streltsov A, Adesso G and Plenio M B 2017 *Rev. Mod. Phys.* **89** 041003
[12] Wang X-L, Yue Q-L, Yu C-H, Gao F and Qin S-J 2017 *Sci. Rep.* **7** 12122
[13] Tan K C, Kwon H, Park C-Y and Jeong H 2016 *Phys. Rev.* A **94** 022329
[14] Southwell K 2008 *Nature* **453** 1003
[15] Wu K-D, Streltsov A, Regula B, Xiang G-Y, Li C-F and Guo G-C 2021 *Adv. Quantum Technol.* **4** 2100040
[16] Guarnieri G, Kolář M and Filip R 2018 *Phys. Rev. Lett.* **121** 070401
[17] Guarnieri G, Morrone D, Çakmak B, Plastina F and Campbell S 2020 *Phys. Lett.* A **384** 126576
[18] Purkayastha A, Guarnieri G, Mitchison M T, Filip R and Goold J 2020 *npj Quantum Inf.* **6** 1
[19] Reppert M, Reppert D, Pachon L A and Brumer P 2020 *Phys. Rev.* A **102** 012211
[20] Cresser J D and Anders J 2021 *Phys. Rev. Lett.* **127** 250601
[21] Román-Ancheyta R, Kolář M, Guarnieri G and Filip R 2021 *Phys. Rev.* A **104** 062209
[22] Cerisola F, Berritta M, Scali S, Horsley S A R, Cresser J D and Anders J 2022 Quantum-classical correspondence in spin-boson equilibrium states at arbitrary coupling (arXiv: 2204.10874 [quant-ph])
[23] Kolář M, Guarnieri G and Filip R 2022 Achieving local coherence in thermal states by intra-system coupling (arXiv: 2211.08851 [quant-ph])
[24] Slobodeniuk A, Novotný T and Filip R 2022 *Quantum* **6** 689
[25] Slobodeniuk A, Novotný T and Filip R 2023 Synthesizing and multiplexing autonomous quantum coherences (arXiv: 2303.07795 [quant-ph])
[26] Etehadi Abari N, Rakhubovsky A and Filip R 2022 *New J. Phys.* **24** 113006
[27] Wang Z, Wu W and Wang J 2019 *Phys. Rev.* A **99** 042320
[28] Brask J B, Clivaz F, Haack G and Tavakoli A 2022 *Quantum* **6** 672

[29] Man Z-X, Tavakoli A, Brask J B and Xia Y-J 2019 *Phys. Scr.* **94** 075101
[30] Naseem M T and Müstecaplıoğlu O E 2022 *Quantum Sci. Technol.* **7** 045012
[31] Morigi G, Eschner J, Cormick C, Lin Y, Leibfried D and Wineland D J 2015 Dissipative quantum control of a spin chain *Phys. Rev. Lett.* **115**
[32] Tavakoli A, Haack G, Brunner N and Brask J B 2020 *Phys. Rev.* A **101** 012315
[33] Cormick C, Bermudez A, Huelga S F and Plenio M B 2013 Dissipative ground-state preparation of a spin chain by a structured environment *New J. Phys.* **15** 073027
[34] Huelga S F, Rivas Á and Plenio M B 2012 Non-Markovianity-assisted steady state entanglement *Phys. Rev. Lett.* **108**
[35] Tan K C and Jeong H 2018 *Phys. Rev. Lett.* **121** 220401
[36] Plenio M B and Huelga S F 2002 Entangled Light from White Noise *Phys. Rev. Lett.* **88**
[37] Treutlein P, Genes C, Hammerer K, Poggio M and Rabl P 2014 *Cavity Optomechanics* (Springer) pp 327–51
[38] Rogers B, Gullo N L, De Chiara G, Palma G M and Paternostro M 2014 *Quantum Meas. Quantum Metrol.* **2** 1
[39] Chu Y and Gröblacher S 2020 *Appl. Phys. Lett.* **117** 150503
[40] Kervinen M, Rissanen I and Sillanpää M 2018 *Phys. Rev.* B **97** 205443
[41] Arrangoiz-Arriola P, Wollack E A, Wang Z, Pechal M, Jiang W, McKenna T P, Witmer J D, Laer R V and Safavi-Naeini A H 2019 *Nature* **571** 537
[42] Bienfait A *et al* 2019 *Science* **364** 368
[43] Bienfait A *et al* 2020 *Phys. Rev.* X **10** 021055
[44] Mirhosseini M, Sipahigil A, Kalaee M and Painter O 2020 *Nature* **588** 599
[45] Ma X, Viennot J J, Kotler S, Teufel J D and Lehnert K W 2021 *Nat. Phys.* **17** 322
[46] Bild M, Fadel M, Yang Y, von Lüpke U, Martin P, Bruno A and Chu Y 2023 *Science* **380** 274
[47] Solki H, Motazedifard A and Naderi M H 2023 *Phys. Rev.* A **108** 063505
[48] Lee D, Lee K W, Cady J V, Ovartchaiyapong P and Jayich A C B 2017 *J. Opt.* **19** 033001
[49] Sohn Y-I *et al* 2018 *Nat. Commun.* **9** 2012
[50] Whiteley S J *et al* 2019 *Nat. Phys.* **15** 490
[51] Marcks J C, Onizhuk M, Wang Y-X, Zhu Y, Jin Y, Soloway B S, Fukami M, Delegan N, Heremans F J, Clerk A A, Galli G and Awschalom D D 2023 Quantum spin probe of single charge dynamics (arXiv: 2312.02894 [cond-mat, physics:quant-ph])
[52] Chen Q, Schwarz I and Plenio M B 2017 Steady-state preparation of long-lived nuclear spin singlet pairs at room temperature *Phys. Rev. B* **95**
[53] Carter S G, Bracker A S, Yakes M K, Zalalutdinov M K, Kim M, Kim C S, Lee B and Gammon D 2019 *Nano Lett.* **19** 6166
[54] Yeo I *et al* 2014 *Nat. Nanotechnol.* **9** 106
[55] Kettler J *et al* 2021 *Nat. Nanotechnol.* **16** 283
[56] Lo H-Y, Kienzler D, de Clercq L, Marinelli M, Negnevitsky V, Keitch B C and Home J P 2015 *Nature* **521** 336
[57] Kienzler D, Flühmann C, Negnevitsky V, Lo H-Y, Marinelli M, Nadlinger D and Home J P 2016 *Phys. Rev. Lett.* **116** 140402
[58] Etehadi Abari N and Naderi M H 2020 *J. Opt. Soc. Am. B* **37** 2146
[59] Argüello-Luengo J and Chang D E 2022 *New J. Phys.* **24** 023006
[60] Bemani F, Roknizadeh R, Motazedifard A, Naderi M H and Vitali D 2019 *Phys. Rev.* A **99** 063814
[61] Allahverdi H, Motazedifard A, Dalafi A, Vitali D and Naderi M H 2022 *Phys. Rev.* A **106** 023107
[62] Xiang Z-L, Ashhab S, You J Q and Nori F 2013 *Rev. Mod. Phys.* **85** 623
[63] Kounalakis M, Blanter Y M and Steele G A 2019 *npj Quantum Inf.* **5** 1
[64] Wollack E A, Cleland A Y, Gruenke R G, Wang Z, Arrangoiz-Arriola P and Safavi-Naeini A H 2022 *Nature* **604** 463
[65] Sohn Y-I, Meesala S, Pingault B, Atikian H A, Holzgrafe J, Gundogan M, Stavrakas C, Stanley M J, Sipahigil A and Choi J 2017 arXiv: 1706.03881
[66] Wang Y K and Hioe F T 1973 *Phys. Rev.* A **7** 831
[67] Kirton P, Roses M M, Keeling J and Dalla Torre E G 2019 *Adv. Quantum Technol.* **2** 1800043
[68] Jacobs K, Nurdin H I, Strauch F W and James M 2015 *Phys. Rev.* A **91** 043812
[69] O'Connell A D *et al* 2010 *Nature* **464** 697
[70] Demkowicz-Dobrzański R, Jarzyna M and Kołodyński J 2015 *Progress in Optics* vol 60ed E Wolf (Elsevier) pp 345–435
[71] Braunstein S L and Caves C M 1994 *Phys. Rev. Lett.* **72** 3439
[72] Demkowicz-Dobrzanski R, Gorecki W and Guta M 2020 (arXiv: 2001.11742 [quant-ph])
[73] Qiao H *et al* 2023 *Science* **380** 1030
[74] Lloyd S 2011 *J. Phys: Conf. Ser.* **302** 012037
[75] Malinovskaya S A and Novikova I 2015 *From Atomic to Mesoscale: The Role of Quantum Coherence in Systems of Various Complexities* (World Scientific)
[76] Lostaglio M, Jennings D and Rudolph T 2015 *Nat. Commun.* **6** 1
[77] Horodecki M and Oppenheim J 2013 *Nat. Commun.* **4** 1
[78] Korzekwa K, Lostaglio M, Oppenheim J and Jennings D 2016 *New J. Phys.* **18** 023045
[79] Santos J P, Céleri L C, Landi G T and Paternostro M 2019 *npj Quantum Inf.* **5** 1
[80] Francica G, Goold J and Plastina F 2019 *Phys. Rev.* E **99** 042105
[81] Van Vu T and Saito K 2022 *Phys. Rev. Lett.* **128** 010602
[82] Rosenfeld E, Riedinger R, Gieseler J, Schuetz M and Lukin M D 2021 *Phys. Rev. Lett.* **126** 250505
[83] Li P-B, Zhou Y, Gao W-B and Nori F 2020 *Phys. Rev. Lett.* **125** 153602
[84] Rusconi C C, Perdriat M, Hétet G, Romero-Isart O and Stickler B A 2022 *Phys. Rev. Lett.* **129** 093605
[85] Garraway B M 2011 *Phil. Trans. R. Soc.* A **369** 1137
[86] Chilingaryan S A and Rodríguez-Lara B M 2013 *J. Phys. A: Math. Theor.* **46** 335301
[87] Peng J, Ren Z, Guo G and Ju G 2012 *J. Phys. A: Math. Theor.* **45** 365302
[88] Peng J, Ren Z, Braak D, Guo G, Ju G, Zhang X and Guo X 2014 *J. Phys. A: Math. Theor.* **47** 265303
[89] Johansson J R, Nation P D and Nori F 2012 *Comput. Phys. Commun.* **183** 1760
[90] Redfield A 1965 Advances in Magnetic and Optical Resonance *Advances in Magnetic Resonance* vol 1 (Elsevier) pp 1–32
[91] Breuer H-P and Petruccione F 2007 *The Theory of Open Quantum Systems* (Oxford University Press)
[92] Hyllus P, Laskowski W, Krischek R, Schwemmer C, Wieczorek W, Weinfurter H, Pezzé L and Smerzi A 2012 *Phys. Rev.* A **85** 022321

[93] Wootters W K 2001 *Quantum Inf. Comput.* **1** 27 (available at: http://www.rintonpress.com/journals/qic-1-1/eof2.pdf)
[94] Plenio M B 2005 *Phys. Rev. Lett.* **95** 090503
[95] Buscemi F and Bordone P 2013 *Phys. Rev.* A **87** 042310
[96] Henderson L and Vedral V 2001 *J. Phys. A: Math. Gen.* **34** 6899
[97] Roses M M and Dalla Torre E G 2020 *PLoS One* **15** e0235197
[98] Tessier T E, Deutsch I H, Delgado A and Fuentes-Guridi I 2003 *Phys. Rev.* A **68** 062316